The medium modification of the charge-weighted Energy-Energy Correlators in Pb+Pb collisions at $\sqrt{s_{NN}}$ = 5.02 TeV*

Han-Yao Liu (刘汉垚)[1#] Shi-Yong Chen (陈时勇)[2,3#] Wei Dai (代巍)[1†]
Ben-Wei Zhang (张本威)[3] Enke Wang (王恩科)[4,5]

[1]School of Mathematics and Physics, China University of Geosciences, Wuhan 430074, China
[2]Huanggang Normal University, Huanggang 438000, China
[3]Key Laboratory of Quark & Lepton Physics (MOE) and Institute of Particle Physics, Central China Normal University, Wuhan 430079, China
[4]State Key Laboratory of Nuclear Physics and Technology, Institute of Quantum Matter, South China Normal University, Guangzhou 510006, China
[5]Guangdong Basic Research Center of Excellence for Structure and Fundamental Interactions of Matter, Guangdong Provincial Key Laboratory of Nuclear Science, Guangzhou 510006, China

Abstract: We report a systematic study and predictions of medium-induced modifications in charge-dependent jet substructure using the charge-weighted Energy-Energy Correlators (EEC) in 0−10% central Pb+Pb collisions at $\sqrt{s_{NN}}$ = 5.02 TeV. Charged-hadron jets, as well as flavor-separated quark- and gluon-initiated jets with momenta of 40−60 GeV and R = 0.4, are analyzed. The ratio of the charge-weighted distribution to the inclusive EEC, which reflects the magnitude of charge correlations, is uniformly negative, demonstrating the dominance of opposite-charge pairs due to charge conservation. A clear flavor dependence is observed: gluon-initiated jets exhibit weaker opposite-charge correlations in the transition and small-$R_{\rm L}$ regions than quark-initiated jets, but stronger opposite-charge correlations at larger $R_{\rm L}$. In Pb+Pb collisions, the A+A-to-p+p ratio for charge correlations exhibits a universal, flavor-independent pattern: jet quenching enhances opposite-charge correlations at small angles while suppressing them at large angles, leading to a steeper $R_{\rm L}$ dependence of charge correlations in A+A and indicating more rapid decorrelation as $R_{\rm L}$ increases. A distinctive V-shaped modification, together with a plateau-like enhancement, appears in the transition and small-$R_{\rm L}$ regions, independent of jet flavor. By factorizing the EEC into the charged-hadron–pair multiplicity and the average energy-weighting distribution, we identify an enhanced but smeared energy weighting of opposite-charge pairs at small $R_{\rm L}$ as the origin of this modification. These observations indicate that medium-induced broadening of parton-level splittings in the hot, dense medium dissociates the charged di-hadron pairs (such as $\pi^+\pi^-$) present in p+p collisions. The plateau-like enhancement of charge correlations is also found to be unrelated to selection-bias effects.

Keywords: jet quenching, jet substructure, heavy ion

DOI: 10.1088/1674-1137/ae62ff **CSTR:** 32044.14.ChinesePhysicsC.50074103

I. INTRODUCTION

In high-energy heavy-ion collisions, a new state of matter—the quark-gluon plasma (QGP)—can be created, whose properties can be indirectly probed through modifications experienced by hard probes traversing it [1−5]. This phenomenon is known as jet quenching. A prominent hard probe comprises high-energy partons, or jets, produced in an initial hard scattering. Their evolution generally proceeds as follows: first, the high-transverse-momentum parton generated in the hard collision carries finite virtuality and undergoes initial splittings in vacuum, described by perturbative QCD via DGLAP evolution [6]. Subsequently, the evolution proceeds to progressively smaller angles through parton showering and eventually becomes nonperturbative as the partons hadronize, after which the resulting hadrons are reconstructed as jets via clustering algorithms.

Studying how jets are modified as they propagate through the QGP has long been a central topic in the

Received 25 January 2026; Accepted 20 April 2026; Accepted manuscript online 21 April 2026

* This work is supported by the National Natural Science Foundation of China (Key Program) (12535010)

† E-mail: weidai@cug.edu.cn

# These authors contributed equally as the first authors

field. In recent years, sustained investigation of jet substructure has deepened our understanding of jet modification and evolution in the hot and dense medium. Jet substructure observables, constructed from final-state hadrons, encode information about parton-shower evolution and hadronization [7]. A class of such observables, specifically designed to constrain nonperturbative processes, has been used to study modifications to the perturbative phase of jet evolution in the medium. Another category of substructure observables enables the separation of perturbative and nonperturbative regimes across the full angular range—particularly shedding light on the hadronization process [8−15]. The two-point energy–energy correlator (EEC) [16−19]. emerges as one such observable and exhibits a distribution separable into three distinct angular regimes: small angles dominated by the free diffusion of hadrons, large angles governed by perturbative parton-shower evolution, and an intermediate transition region between them [20−27]. In recent years, the EEC has been explored from multiple aspects as a probe of jet quenching phenomena [28−50]. In heavy-ion collisions, it further provides insights into initial-state cold nuclear matter effects [28−32], parton energy-loss mechanisms [33, 34], medium response [35−37], the properties of in-medium light-flavor quarks [34, 38], mass effects in the in-medium evolution of heavy-flavor quarks [24, 32, 39, 40], and the physical properties of the quark-gluon plasma (QGP) [25, 41−50].

Refs. [51, 52] categorize the EEC by considering hadron pairs carrying like or opposite charges, enabling the study of charge correlations during hadronization and providing constraints on hadronization models. This is achieved by including the charge product in the energy weighting, yielding the charge-weighted EEC. Furthermore, the ratio of the charge-weighted EEC to the inclusive EEC offers a reweighted measure of charge correlations as a function of hadron-pair angular separation. These observables have garnered significant attention from experimental collaborations such as STAR and ALICE [21, 53]. Owing to their sensitivity to timescale separation within jets, a detailed investigation of the modification patterns of these observables in A+A collisions is essential. Such studies not only help probe and track jet evolution in the hot and dense medium [24, 54−56], but also establish a valuable baseline for future exploration of hadronization mechanisms in heavy-ion collisions, both theoretically and experimentally.

In this work, we present, in Section II, the theoretical baseline obtained with PYTHIA and compare it with experimental results from RHIC and the LHC. In Section III, we provide, for the first time, theoretical predictions for the charge-weighted EEC distribution of charged-hadron jets with 40−60 GeV and R = 0.4 in 0−10% central Pb+Pb collisions, and discuss the observed jet quenching effects. In Section IV, we compute theoretical predictions for the $R_{\rm L}$ distribution, the ratio of the charge-weighted EEC to the inclusive EEC, and analyze the influence of the medium on the magnitude of charge correlations as a function of the particle-pair angle. Finally, in Section V, we summarize our conclusions and outline future perspectives.

II. p+p BASELINE

The charge-weighted EEC for final-state charged hadrons within jets is constructed in the same way as in previous studies [22, 34], but incorporates the product of the hadron-pair charges into the energy weighting [21]. Experimentally, it is defined as follows:

$$\begin{aligned} &Charge-weighted\ EEC \\ &=\frac{1}{N_{\rm jet}\cdot\Delta R}\int_{R_{\rm L}-\frac{1}{2}\Delta R}^{R_{\rm L}+\frac{1}{2}\Delta R}\sum_{\rm jets}\sum_{i,j}\frac{Q_iQ_jp_{T,i}p_{T,j}}{p_{T,\rm jet}^2}\delta(R_{\rm L}-R_{{\rm L},ij}){\rm d}R_{\rm L} \\ &=EEC_{\rm like}-EEC_{\rm opposite}, \end{aligned} \tag{1}$$

where i and j denote two particles within a jet; $R_{L,ij}=\sqrt{(\phi_j-\phi_i)^2+(\eta_j-\eta_i)^2}$ is their angular separation; Q_i and Q_j are their electric charges; and $p_{T,i}/p_{T,\rm jet}$ and $p_{T,j}/p_{T,\rm jet}$ are their transverse-momentum fractions relative to the jet. ΔR is the angular bin width, and $N_{\rm jet}$ is the total number of jets. This definition naturally separates the EEC into two components: one constructed using only like-charge pairs and one using only opposite-charge pairs. When accounting for the sign of the charge product Q_iQ_j, the charge-weighted EEC corresponds to the contribution from like-charge pairs minus the contribution from opposite-charge pairs. The EEC without considering the charges of particle pairs, as discussed earlier, is the sum of these two contributions. To distinguish it from the charge-weighted EEC, we refer to it as the inclusive EEC hereafter. In addition, the jets in this definition are all reconstructed from final-state charged hadrons, and we will refer to them as charged jets hereafter.

To provide a fair p+p baseline for the jet-quenching study, we used the Monte Carlo event generator PYTHIA v8.313 [57] to simulate p+p collisions at the LHC energy $\sqrt{s}=5.02$ TeV with the default tune [58] and at the RHIC energy $\sqrt{s}=200$ GeV with the Detroit tune [59], matching the STAR Collaboration implementation in [21]. Details are summarized here: Jets were reconstructed using the anti-k_T algorithm from the FastJet v3.4.0 package [60], with a jet radius parameter R = 0.4. At $\sqrt{s}=200$ GeV, we select jets with transverse momenta 20 GeV/c < $p_{\rm T,jet}$ < 30 GeV/c, jet rapidity $|\eta_{\rm jet}|$ < 0.6, composed of charged particles with $p_{T,\rm had}>0.2$ GeV/c. At $\sqrt{s}=5.02$ TeV, we select jets with transverse

momenta 40 GeV/c < $p_{\mathrm{T,jet}}$ < 60 GeV/c, jet rapidity $|\eta_{\mathrm{jet}}| < 0.5$, composed of charged particles with $p_{T,\mathrm{had}} > 1$ GeV/c. To facilitate the subsequent discussion, we define the R_{L} intervals used in this study as follows: we denote $R_{\mathrm{L}} < 0.05$ as small angles dominated by free diffusion of hadrons, $R_{\mathrm{L}} > 0.2$ as large angles governed by perturbative parton-shower evolution, and the intermediate region $0.05 < R_{\mathrm{L}} < 0.2$ as the transition region.

We computed, in p+p collisions at both $\sqrt{s} = 200$ GeV and 5.02 TeV, the distributions of the charge-weighted EEC (upper panel of Fig. 1) and the ratio of the charge-weighted EEC to the inclusive EEC (lower panel). The like-charge component (dashed line), the opposite-charge component (dash-dotted line), and the inclusive EEC distributions (solid line) are plotted together for each collision energy. They are consistent with simulations by the experimental collaborations and also align with the ALICE [53] and STAR experimental data [21]. We find that, for both cases, the like-charge components agree well with the experimental data across the entire R_{L} range. The opposite-charge component underestimates the experimental data at larger R_{L} and overestimates it at smaller R_{L}. Its peak is shifted toward smaller angles, causing the inclusive distribution to shift to larger angles and to overpredict the experimental data at smaller R_{L}. Please note that the ALICE experimental data points shown here are preliminary results, and the data points in the ratio in the lower panel are also derived from these preliminary results.

In the lower panel of Fig. 1, we present the ratio of the charge-weighted distribution to the inclusive EEC at two collision energies, 200 GeV and 5.02 TeV. As suggested in [21], this ratio quantifies the magnitude of charge correlations across the full range from –1 to +1. For the jets in the kinematic range studied, the distribution is concentrated at negative values. A ratio of zero corresponds to the extreme scenario of an infinite thermal bath, where the probabilities of forming like-charge and opposite-charge pairs are equal. However, within our studied range (with an average jet charge $Q = 0.006$ and limited particle numbers within a jet), the opposite-charge correlations are stronger than the like-charge correlations, both overall and predominantly —a consequence of charge conservation. This observable reflects the relative abundance of these two types of correlations as a function of relative angular distance (R_{L}), with more negative values corresponding to stronger correlations of opposite-charge pairs.

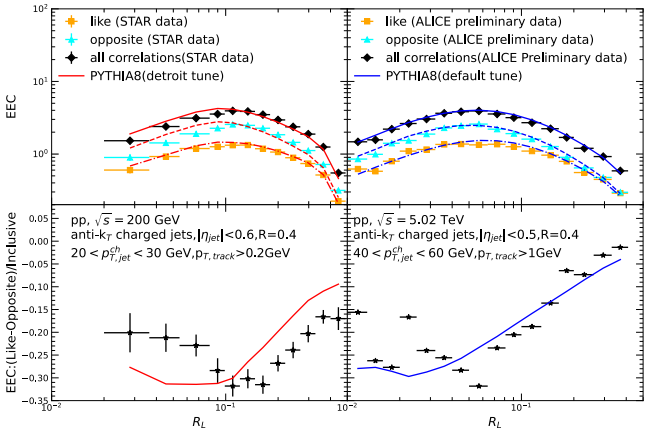

Fig. 1. (color online) PYTHIA 8 simulation results for the normalized charge-weighted EEC, together with its like-charge and opposite-charge components (upper panels), and for the ratio of the charge-weighted to inclusive EEC distributions (lower panels), are presented as functions of R_{L} for inclusive charged jets with a jet size of $R = 0.4$ produced in p + p collisions at $\sqrt{s} = 200$ GeV (left panel) and $\sqrt{s} = 5.02$ TeV (right panel). The results are compared with STAR [21] and ALICE [53] experimental data, respectively.

The mechanism of vacuum hadronization remains an open question; the EEC observables provide valuable constraints on this. STAR and ALICE have also noted in their reports that neither PYTHIA's string-fragmentation mechanism nor Herwig's cluster mechanism can explain this phenomenon. In this paper, we do not intend to explore or attempt to resolve this issue. Our only concern is whether such a p+p baseline affects our study of the nuclear modification effects for this observable. The answer is no. This is because, in the high-transverse-momentum region, jet-quenching effects are typically factorized into parton-level modifications in the hot, dense medium and the hadronization process in vacuum outside the `fireball', and our calculations are performed precisely in this manner. Under this assumption, we attempt to isolate and study the jet-quenching effects for this observable, thereby laying the foundation for subsequent investigations into the hadronization mechanism in the hot and dense medium. Therefore, in the following sections of the paper, we continue to use the PYTHIA description as the pp baseline for the A+A/pp ratio, and also use the parton-level events generated by PYTHIA as input for the transport model.

III. Charge-weighted EEC IN Pb+Pb COLLISIONS

In this work, we examine the impact of jet quenching on charge correlations, as revealed by the ratio of the charge-weighted EEC to the inclusive EEC, using a two-step approach. We first compute the A+A-to-p+p ratio of the charge-weighted EEC within the same transverse-momentum interval as the p+p baseline.

We have developed an updated Monte Carlo framework, primarily based on a Langevin transport equation, to simulate the energy-loss processes of partons produced in initial hard scatterings as they traverse the Quark-Gluon Plasma (QGP) in heavy-ion collisions, referred to as the SHELL model. It incorporates three key physical processes: elastic collisional energy loss, in-medium gluon radiation, and medium response. This model has successfully described a wide range of experimental observables, including those related to jet quenching [61−66].

The model initializes the dynamical distribution of partons using a Glauber-model-based nuclear geometry [67]. These partons are then propagated step by step through a QGP medium whose evolution is governed by relativistic hydrodynamics. At each evolution time step Δt, a parton may simultaneously undergo elastic scattering, radiate gluons, and induce a medium response. The elastic energy loss per unit length is calculated using the Hard Thermal Loop (HTL) formula [68]:

$$\frac{\mathrm{d}E}{\mathrm{d}t} = \frac{\alpha_s C_s}{2}\mu_D^2 \ln\left(\frac{\sqrt{ET}}{\mu_D}\right), \tag{2}$$

where α_s is the running coupling constant of the strong interaction, taken to be 0.3 in our calculations; C_s is the Casimir operator ($C_A = 3$ for a gluon, $C_F = 4/3$ for a quark); μ_D is the Debye screening mass; and E and T are the parton energy and the local medium temperature, respectively.

The energy deposited into the medium via these elastic collisions accumulates within and interacts with the QGP, eventually hadronizing at freeze-out to form "wake" particles. This constitutes the medium-response mechanism in SHELL. The momentum distribution of these wake hadrons is computed using the Cooper-Frye prescription including perturbations [69, 70]:

$$\begin{aligned} E\frac{\mathrm{d}\Delta N}{\mathrm{d}^3 p} =& \frac{1}{32\pi}\frac{m_T}{T^5}\cosh(y-y_j)\exp\left[-\frac{m_T}{T}\cosh(y-y_j)\right] \\ &\times\left\{p_T\Delta P_T\cos(\phi-\phi_j)\right. \\ &\left.+\frac{1}{3}m_T\Delta M_T\cosh(y-y_j)\right\}, \end{aligned} \tag{3}$$

Here, E, $\boldsymbol{p}$, ΔN, m_T, p_T, y, and ϕ denote the energy, momentum, yield, transverse mass, transverse momentum, rapidity, and azimuthal angle of the wake hadron, respectively. y_j and ϕ_j denote the rapidity and azimuthal angle of the energy-depositing parton. ΔP_T and $\Delta M_T = \Delta E/\cosh(y_j)$ represent the transverse momentum and transverse mass transferred to the medium, where ΔE is the accumulated deposited energy. The first and second terms on the right-hand side correspond to the momentum and energy of the wake hadrons, respectively.

Within SHELL, the probability that a parton radiates a gluon during a time step Δt in the QGP is given by:

$$P_{\mathrm{rad}}(t,\Delta t) = 1 - \mathrm{e}^{-\langle N(t,\Delta t)\rangle}, \tag{4}$$

where $\langle N(t,\Delta t)\rangle$ denotes the average number of radiated gluons, obtained from the medium-induced gluon spectrum within the higher-twist (HT) formalism [71−74]:

$$\frac{\mathrm{d}N}{\mathrm{d}x\,\mathrm{d}k_\perp^2\,\mathrm{d}t} = \frac{2\alpha_s C_s P(x)\hat{q}}{\pi k_\perp^4}\sin^2\left(\frac{t-t_i}{2\tau_f}\right)\left(\frac{k_\perp^2}{k_\perp^2+x^2M^2}\right)^4, \tag{5}$$

Here, $k_\perp$ is the transverse momentum of the radiated gluon; $x = E_g/E_p$ is the energy fraction of the gluon relative to the parent parton; M is the mass of the parent parton; $P(x)$ is the vacuum QCD splitting function; $\tau_f = 2Ex(1-x)/(k_\perp^2 + x^2M^2)$ is the gluon formation time; $t - t_i$ is the time interval in the parton frame; and $\hat{q} = \hat{q}_0(T/T_0)^3 p_\mu u^\mu$ is the jet transport parameter, where $\hat{q}_0 = 1.5\ \mathrm{GeV}^2/\mathrm{fm}$, u^μ is the four-velocity of the QGP at the given space-time point, and T_0 is the initial temperature. This transport parameter is the key dynamical quantity governing the strength of parton energy loss. The number of radiated gluons in a given step is sampled from a Poisson distribution, and their four-momenta are subsequently calculated.

The space-time evolution of the expanding QGP fireball is provided by the (3+1)-dimensional CLVisc hydrodynamic model [75]. The hadronization temperature is set to $T_c = 165$ MeV; partons, as well as the deposited wake energy, are hadronized once the local temperature falls below this value. Final-state hadrons are obtained by first forming color-singlet strings using the colorless method from the JETSCAPE collaboration [76], followed by hadronization and hadron decays via the PYTHIA Lund string model.

Based on Eq. (2), we note that the charge-weighted EEC is numerically equivalent to the like-charge component minus the opposite-charge component of the inclusive EEC. Our previous work [34] further demonstrated that the in-medium modification of the EEC exhibits distinct behaviors for gluon- and quark-initiated jets. We present in Fig. 2 the charge-weighted EEC distributions in p+p and A+A (upper panel) and their A+A/p+p ratios (lower panel) for inclusive charged jets, quark-initiated jets, and gluon-initiated jets in central (0−10%)

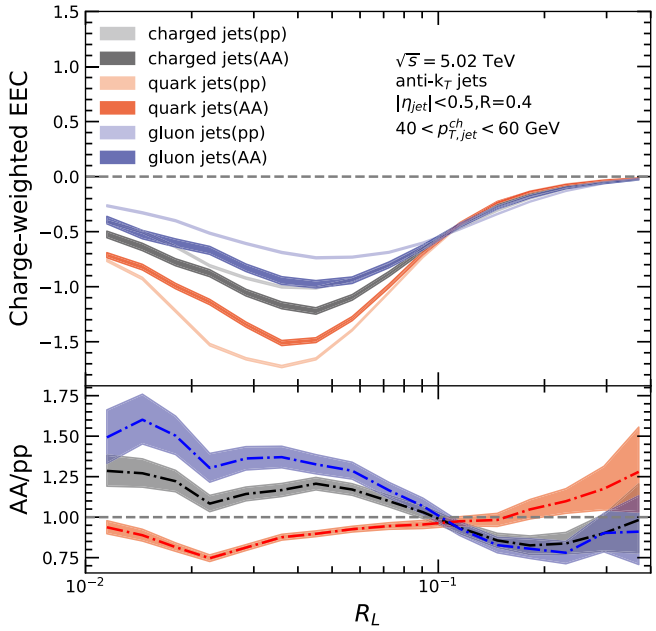

Fig. 2. (color online) Charge-weighted EEC in p+p and central (0−10%) Pb+Pb collisions, and the corresponding A+A/p+p ratio distributions, with statistical uncertainties, shown as functions of $R_{\rm L}$ for inclusive charged, gluon, and quark jets with radius R = 0.4 in the jet p_T interval 40−60 GeV at $\sqrt{s}$ = 5.02 TeV.

Pb+Pb collisions at $\sqrt{s_{NN}}$ = 5.02 TeV. All jets are reconstructed from charged particles with $p_{T,\rm had} > 1$ GeV/c using the anti-k_T algorithm with a radius parameter of R = 0.4, and are selected with transverse momentum in the range 40−60 GeV/c and pseudorapidity $|\eta^{\rm jet}| < 0.5$. Variations of the jet transport parameter and the hadronization threshold temperature within their uncertainty ranges lead to only minor changes in the $R_{\rm L}$ distribution and do not significantly alter the main features of its A+A/p+p ratio. The figure also displays the statistical-uncertainty bands. In the subsequent discussion of the underlying mechanisms, we will adopt fixed values of the transport parameter and hadronization threshold temperature consistent with our previous work, including Ref. [34].

In the p+p system, the charge-weighted EEC distribution lies predominantly in the negative region under the studied conditions, indicating that opposite-charge pairs contribute more than like-charge pairs. Beyond the transition region toward larger $R_{\rm L}$, the distribution exhibits a positive slope. In contrast, toward smaller $R_{\rm L}$ it shows a negative slope—that is, the difference between opposite- and like-charge contributions decreases as $R_{\rm L}$ decreases. Regarding flavor dependence, the charge-weighted distribution of gluon-initiated jets lies closer to zero than that of quark-initiated jets. In the small-$R_{\rm L}$ region, the difference between opposite- and like-charge pairs is significantly smaller in gluon jets than in quark jets, while in the large-$R_{\rm L}$ region, this difference becomes slightly larger in gluon jets than in quark jets. In A+A, we observe that the behavior of the A+A/p+p ratios resembles the previously reported modification of the EEC in a hot, dense medium, with characteristic modification patterns for quark and gluon jets also being consistent [34]. This suggests a common modification mechanism for the EEC distributions: the enhancement in the small-$R_{\rm L}$ region is dominated by selection bias and the initial spectral properties of gluon jets, while the suppression at larger $R_{\rm L}$ that increases with $R_{\rm L}$ is primarily driven by broadening effects due to radiative energy loss. Notably, in the small-$R_{\rm L}$ region around $R \approx 0.02$, we observe a characteristic V-shaped modification pattern. To further investigate the origin of this feature, it is necessary to examine the medium modifications of the like-charge and opposite-charge components separately.

In Fig. 3, we present the distributions of the like-charge and opposite-charge components in p+p and A+A collisions (upper panel), with their corresponding A+A to p+p ratios shown in the bottom panel. While their modification patterns are generally similar to those of the inclusive EEC, the opposite-charge component exhibits a stronger enhancement in both the transition region and at small $R_{\rm L}$ compared with the like-charge component. Moreover, the V-shaped modification structure at small $R_{\rm L}$ is found exclusively in the opposite-charge component. This is consistent with the pattern observed in the charge-weighted EEC at small $R_{\rm L}$.

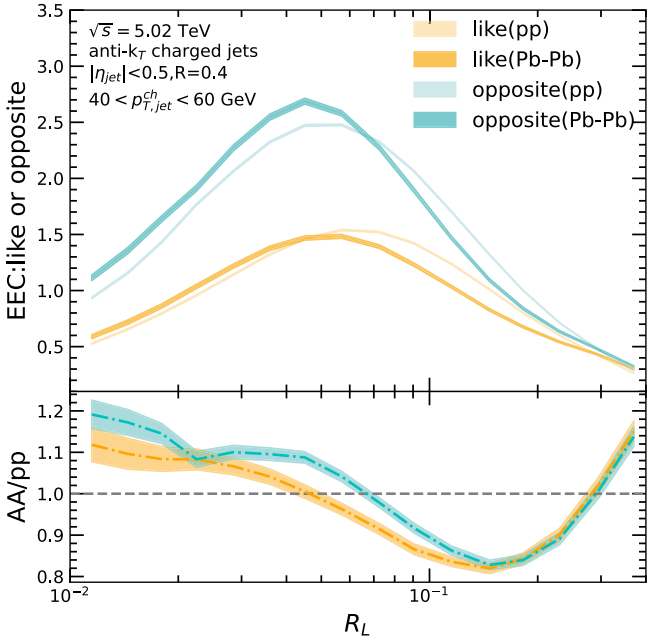

Fig. 3. (color online) The like and opposite components of the EEC in p+p and central (0−10%) Pb+Pb collisions, and the distributions of their A+A/p+p ratios with statistical uncertainties, as functions of $R_{\rm L}$ for inclusive charged jets with radius R = 0.4 at $\sqrt{s}$ = 5.02 TeV in the jet $p_{\rm T}$ interval 40 – 60 GeV.

To further investigate the raw charge correlations without energy weighting and to understand how jet quenching manifests, we adopt the same methodology as in previous work [34]: we factorize the EEC distribution into the distribution of the average number of final-state charged hadron pairs per jet as a function of $R_{\rm L}$ and the corresponding average energy-energy weighting of hadron pairs within each $R_{\rm L}$ bin, ⟨weight⟩. The hadron pairs can then be categorized as like-charge or opposite-charge. We therefore decompose the EEC distribution for the like-charge and opposite-charge components as follows:

$$\Sigma_{\rm EEC}^{\rm comp} = \frac{N_{\rm pair}^{\rm total}}{N_{\rm jet}} \cdot \frac{\Delta N_{\rm pair}^{\rm comp}}{N_{\rm pair}^{\rm total}\Delta R} \cdot \langle {\rm weight} \rangle^{\rm comp}, \tag{6}$$

where $N_{\rm pair}^{\rm total}$ is the total number of particle pairs, $\Delta N_{\rm pair}$ is the number of pairs within an angular bin of width ΔR centered at R, and ⟨weight⟩ represents the average energy weight carried by the pairs in that bin.

In the upper panel of Fig. 4, the $R_{\rm L}$ distributions of like-charge and opposite-charge hadron pairs in p+p collisions are shown as solid lines. Without energy weighting, the raw hadron pairs are predominantly distributed at large $R_{\rm L}$ values. As required by charge conservation, the number of opposite-charge pairs exceeds that of like-charge pairs across the entire $R_{\rm L}$ range. In A+A collisions, the $R_{\rm L}$ distributions of both types of hadron pairs shift toward larger $R_{\rm L}$. The suppression of opposite-charge pairs at small angles is slightly weaker than that of like-charge pairs, and the enhancement at large angles is also somewhat milder for opposite-charge pairs. In the lower panel of Fig. 4, we observe that the average energy weighting of opposite-charge pairs is significantly larger than that of like-charge pairs in both the transition region and at small $R_{\rm L}$. Although this difference becomes modest at large $R_{\rm L}$, it is compounded by the contrasting angular distributions of hadron pairs in this region. In the A+A case, opposite-charge pairs exhibit a stronger enhancement relative to p+p collisions at small $R_{\rm L}$ than do like-charge pairs, whereas the suppression at large $R_{\rm L}$ is nearly identical for both types. Notably, a characteristic V-shaped modification pattern emerges in the opposite-charge component, manifested as a pronounced enhancement in the small-$R_{\rm L}$ region. This can be identified as the underlying origin of the analogous modification pattern observed in the charge-weighted EEC. We also analyzed this phenomenon by separating different jet quenching mechanisms and found that, whether it is elastic energy loss, inelastic energy loss, or medium excitation processes, the dip appears at the same $R_{\rm L}$, suggesting that it is not caused by any specific jet quenching mechanism.

Calculating the charge-weighted EEC for a more specific hadronization channel, such as $\pi^+\pi^-$ pairs, and its A+A/pp ratio yields a much clearer valley structure than

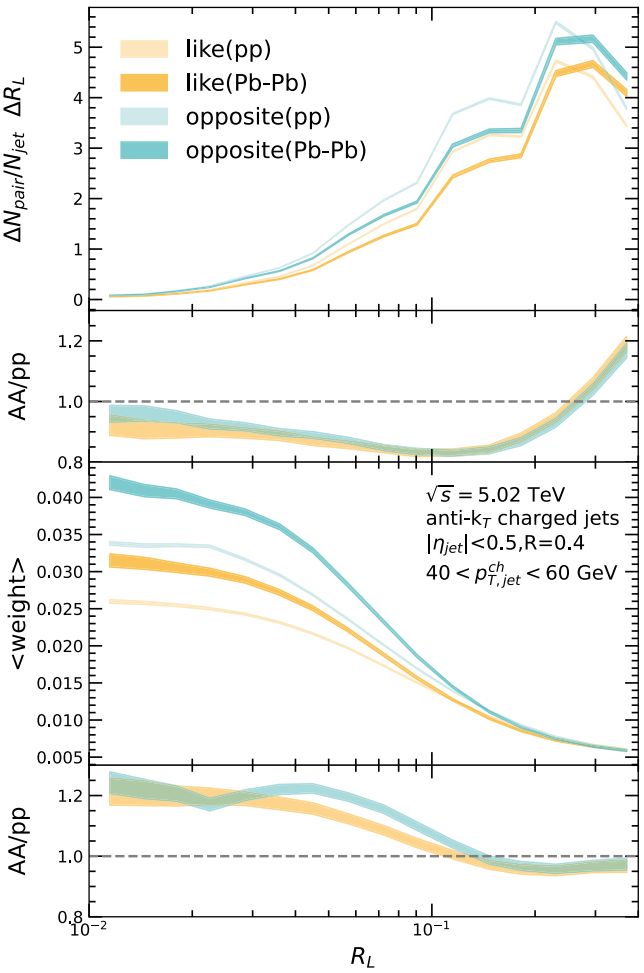

Fig. 4. (color online) Per-jet normalized pair-number distributions (upper panel) and average energy-weight distributions (lower panel), with statistical uncertainties, for the like and opposite components of the EEC in p+p and central (0−10%) Pb+Pb collisions, and the corresponding A+A/p+p ratios, shown as functions of $R_{\rm L}$ for inclusive charged jets with radius R = 0.4 at $\sqrt{s}$ = 5.02 TeV in the jet p_T interval 40 – 60 GeV.

the results in the bottom panel of Fig. 3. For the $\pi^+\pi^-$ pair channel, the more pronounced bump in the energy-weighting distribution in pp collisions (similar to that shown in the lower panel of Fig. 4) is smeared out in A+A collisions, resulting in a larger dip in its A+A/pp ratio. This indicates that the underlying physical mechanism is parton-level splitting broadening induced by the hot, dense medium, which causes charged di-hadron pairs like $\pi^+\pi^-$ that are present in pp collisions to be dissociated in A+A collisions.

IV. charge-weighted EEC/INCLUSIVE EEC RATIOS IN Pb+Pb COLLISIONS

Finally, we turn to the interpretation of the ratio

between the charge-weighted distribution and the inclusive EEC. As noted earlier, this ratio quantitatively characterizes the degree of charge correlation, allowing us to focus specifically on correlations among hadron pairs. Because the $R_{\rm L}$ variable of the EEC observable can be used to infer the jet formation process in reverse, Fig. 1 shows that, as the jet evolves from the large-$R_{\rm L}$ region—dominated by QCD shower processes—toward the transition region, opposite-charge correlations strengthen relative to like-charge ones. Moving further into the hadronization stage (from the transition toward small $R_{\rm L}$), where hadron pairs form at the smallest angular separations, opposite-charge correlations are strongest. We now assess the impact of jet quenching on these charge correlations.

In Fig. 5, we present the charge correlations and their A+A/p+p ratios for charged-hadron jets, gluon-initiated jets, and quark-initiated jets with a momentum of 40−60 GeV and R = 0.4 in 0−10% Pb+Pb collisions at 5.02 TeV. In the p+p baseline, the slope of the charge correlations as a function of $R_{\rm L}$ is steeper for quark jets than for gluon jets. Consequently, quark jets exhibit faster opposite-charge decorrelation at large $R_{\rm L}$ while showing the strongest opposite-charge correlations at small $R_{\rm L}$. The A+A/p+p ratios for all three jet types display a consistent modification pattern: a plateau-like enhancement in the transition and small-$R_{\rm L}$ region and a suppression that increases with $R_{\rm L}$ in the large-$R_{\rm L}$ region. This demonstrates that jet quenching reduces opposite-charge correlations at large $R_{\rm L}$ while enhancing them in the transition and small-$R_{\rm L}$ region, resulting in an increased slope of the charge correlations with $R_{\rm L}$. Two important observations emerge. First, the characteristic modification patterns that distinguish quark jets from gluon jets in the charge-weighted EEC and inclusive EEC are canceled when taking their ratio. Second, the distinctive V-shaped medium modification observed in the A+A/p+p ratio of the opposite-charge component of the charge-weighted EEC appears at the same $R_{\rm L}$ position, independent of the jet-initiator flavor.

From the analysis in Fig. 2, we observe that the jet-quenching modification patterns for charged EEC (like-opposite) of quark jets and gluon jets are highly consistent with those for EEC (opposite+like), as their modifications are predominantly governed by the energy-weighting correction. Furthermore, the component-wise analysis in Fig. 3 and Fig. 4 reveals that both the opposite component and the like component exhibit modification patterns in the same direction. Consequently, the charge correlations, represented by (like-opposite)/(opposite+like), tend to cancel out the characteristic modification patterns present in both the charged EEC and the inclusive EEC for quark jets and gluon jets. Therefore, it is justified to conclude that the redistribution of charge correlations is independent of the initiator's color charge.

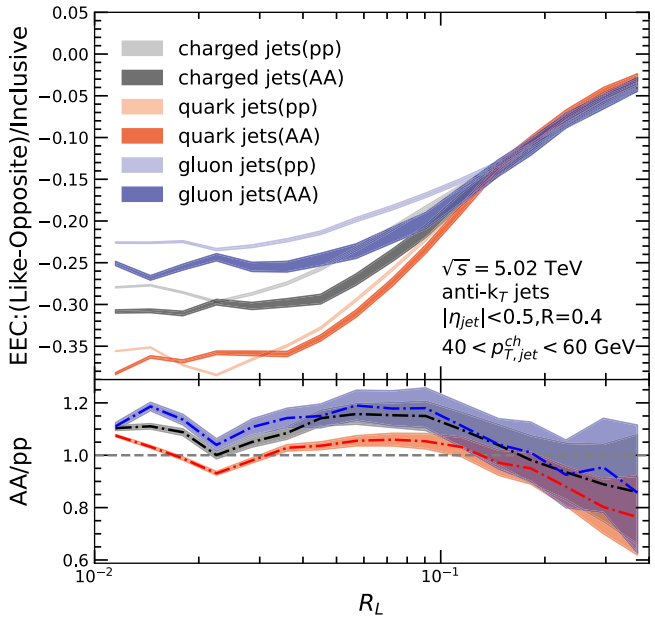

Fig. 5. (color online) Charge-weighted EEC-to-inclusive EEC ratios in p+p and central (0−10%) Pb+Pb collisions, and the corresponding A+A/p+p ratio distributions, shown with statistical uncertainties as functions of $R_{\rm L}$, for inclusive charged, gluon, and quark jets with radius R = 0.4 in the jet p_T interval 40 – 60 GeV at $\sqrt{s}$ = 5.02 TeV.

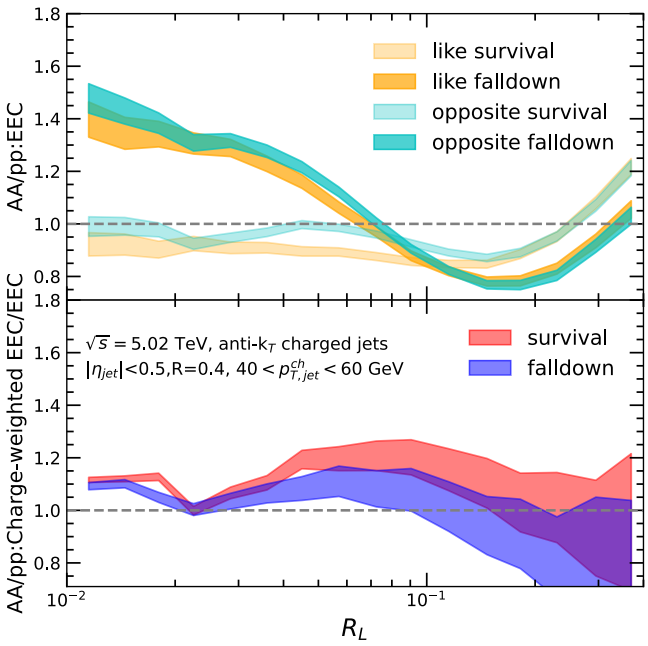

Fig. 6. (color online) *survival* and *fall-down* contributions to the A+A/p+p ratios of the like-charge and opposite-charge components of the EEC (upper panel) and to the charge-weighted EEC/inclusive EEC (bottom panel) in central (0−10%) Pb+Pb collisions, with statistical uncertainties, as functions of $R_{\rm L}$ for inclusive charged jets with a radius of R = 0.4 in the jet p_T interval 40−60 GeV at $\sqrt{s_{NN}}$ = 5.02 TeV.

Next, we examine whether the plateau-like enhancement of charge correlations in the transition and small-$R_{\rm L}$ region is related to selection bias, since such an effect dominates the enhancement of the inclusive EEC in the small-$R_{\rm L}$ region. Can it be canceled in this ratio? We plot in Fig. 6 (upper panel) the separate contributions of the *survival* and *fall-down* mechanisms to the A+A/p+p ratio for both like-charge and opposite-charge components, while the lower panel compares their impacts on the A+A/p+p ratio of the charge correlations. Here, *survival* denotes jets in A+A collisions whose corresponding progenitor jets in p+p collisions fall within the same momentum interval, whereas *fall-down* refers to A+A jets originating from p+p jets initially at higher momentum. In the decomposed view (upper panel), the effects of both mechanisms on the A+A/p+p ratio are consistent with our earlier EEC results—the *fall-down* contribution enhances the distribution in the small-$R_{\rm L}$ region. However, the lower panel reveals that the overall behaviors of the *survival* and *fall-down* cases are qualitatively similar, with only a minor difference in the small-$R_{\rm L}$ region. At large $R_{\rm L}$, the *fall-down* contribution induces a more rapid decorrelation as $R_{\rm L}$ increases. We therefore conclude that the plateau-like enhancement of the charge correlations in the transition and small-$R_{\rm L}$ region is unrelated to selection bias, as this effect is canceled by constructing the ratio.

V. SUMMARY

This work presents a systematic investigation of medium modifications to the charge-dependent jet substructure using the charge-weighted EEC in p+p and 0−10% central Pb+Pb collisions at $\sqrt{s_{NN}} = 5.02$ TeV. We analyze charged-hadron jets along with flavor-separated quark- and gluon-initiated jets in the 40−60 GeV momentum range with $R = 0.4$. In p+p collisions, the charge correlations are consistently negative, reflecting the dominance of opposite-charge pairs due to charge conservation. In the transition and large $R_{\rm L}$ regions, opposite-charge pairs exhibit progressively stronger decorrelation as $R_{\rm L}$ increases. While PYTHIA simulations predict that opposite-charge correlations reach their maximum in the small-$R_{\rm L}$ region and then remain approximately constant, they fail to describe the experimentally observed decorrelation behavior as $R_{\rm L}$ increases. Meanwhile, a clear flavor dependence emerges: gluon-initiated jets exhibit weaker opposite-charge correlations in the transition and small-$R_{\rm L}$ regions than quark-initiated jets, but stronger correlations in the large-$R_{\rm L}$ region.

In Pb+Pb collisions, significant medium modifications are observed. A detailed calculation of the A+A/p+p ratio for the charge-weighted EEC reveals a modification pattern highly consistent with that of the inclusive EEC. A distinctive V-shaped modification appears exclusively in the opposite-charge component of the charge-weighted EEC, occurring at the same $R_{\rm L}$ position regardless of jet flavor. By factorizing the EEC into the charged-hadron pair multiplicity and the average energy-weighting distributions as functions of $R_{\rm L}$, we find that the enhanced but smeared energy weighting of opposite-charge pairs at small $R_{\rm L}$ is the origin of the observed modification. This indicates that the phenomenon stems from medium-induced broadening of parton splittings, which leads to the dissociation of dihadron ($\pi^+\pi^-$) pairs in A+A collisions, rather than their survival as in the p+p baseline.

The A+A/p+p ratio for charge correlations shows a universal pattern across all jet types: a plateau-like enhancement in the transition and small-$R_{\rm L}$ regions, and increasing suppression with $R_{\rm L}$ in the large-$R_{\rm L}$ region. Jet quenching enhances opposite-charge correlations at small angles while reducing them at large angles, resulting in a steeper $R_{\rm L}$ dependence and a more rapid decorrelation with increasing $R_{\rm L}$. The flavor dependence appears to cancel when taking the ratio of the charge-weighted distribution to the inclusive EEC. The distinctive V-shaped modification, which appears exclusively in the opposite-charge component of the charge-weighted EEC, occurs at the same $R_{\rm L}$ position regardless of jet flavor. The plateau-like enhancement of charge correlations in the transition and small-$R_{\rm L}$ regions is unrelated to selection-bias effects, based on the analysis of survival and fall-down contributions.

Our results establish charge-sensitive correlators as a powerful tool for probing jet-quenching mechanisms and the redistribution of charge correlations within jets in the quark-gluon plasma, and pave the way to further constrain hadronization mechanisms in the hot QCD medium.

References

[1] M. Gyulassy and M. Plumer, Phys. Lett. B **243**, 432 (1990)
[2] X. Luo and N. Xu, Nucl. Sci. Tech. **28**, 112 (2017), arXiv: 1701.02105[nucl-ex]
[3] Z. Tang, Z.-B. Tang, W. Zha *et al.*, Nucl. Sci. Tech. **31**, 81 (2020), arXiv: 2105.11656[nucl-ex]
[4] H.-X. Zhang, Y.-X. Xiao, J.-W. Kang *et al.*, Nucl. Sci. Tech. **33**, 150 (2022), arXiv: 2102.11792[hepph]
[5] Q.-Y. Shou, Y.-G. Ma, S. Zhang *et al.*, Nucl. Sci. Tech. **35**, 219 (2024), arXiv: 2409.17964[nucl-ex]
[6] S. Höche, F. Krauss, and S. Prestel, JHEP **10**, 093 (2017), arXiv: 1705.00982[hep-ph]
[7] M. Aaboud, G. Aad, B. Abbott *et al.*, Phys. Rev. C **98**, 024908 (2018), arXiv: 1805.05424[nucl-ex]
[8] A. J. Larkoski, I. Moult, and B. Nachman, Phys. Rept. **841**, 1 (2020), arXiv: 1709.04464[hep-ph]
[9] Y.-F. Liu, W. Dai, B.-W. Zhang *et al.*, Chin. Phys. C **49**,

044108 (2025), arXiv: 2205.14668[hep-ph]
[10] Q. Zhang, Z.-X. Xu, W. Dai *et al*., arXiv: 2303.08620[nucl-th]
[11] R. Kogler *et al*., Rev. Mod. Phys. **91**, 045003 (2019), arXiv: 1803.06991[hep-ex]
[12] W. Dai, I. Vitev, and B.-W. Zhang, Phys. Rev. Lett. **110**, 142001 (2013), arXiv: 1207.5177[hep-ph]
[13] W. Dai, S. Wang, S.-L. Zhang *et al*., Chin. Phys. C **44**, 104105 (2020), arXiv: 1806.06332[nucl-th]
[14] T. Luo, S. Cao, Y. He *et al*., Phys. Lett. B **782**, 707 (2018), arXiv: 1803.06785[hep-ph]
[15] S. Wang, W. Dai, B.-W. Zhang *et al*., Eur. Phys. J. C **79**, 789 (2019), arXiv: 1906.01499[nucl-th]
[16] C. L. Basham, L. S. Brown, S. D. Ellis *et al*., Phys. Rev. D **17**, 2298 (1978)
[17] C. L. Basham, L. S. Brown, S. D. Ellis *et al*., Phys. Rev. Lett. **41**, 1585 (1978)
[18] C. L. Basham, L. S. Brown, S. D. Ellis *et al*., Phys. Rev. D **19**, 2018 (1979)
[19] C. Berger, H. Genzel, W. Lackas *et al*.(PLUTO Collaboration), Z. Phys. C **28**, 365 (1985)
[20] H. Chen, I. Moult, X. Zhang *et al*., Phys. Rev. D **102**, 054012 (2020), arXiv: 2004.11381[hep-ph]
[21] B. E. Aboona *et al*., Phys. Rev. Lett. **135**, 111901 (2025), arXiv: 2502.15925[hep-ex]
[22] S. Acharya *et al*. (ALICE), arXiv: 2409.12687 [hep-ex]
[23] S. Acharya *et al*. (ALICE), arXiv: 2504.03431[hep-ex]
[24] M. Mazzilli (ALICE), PoS EPS-HEP **2023**, 262 (2024)
[25] B. Liang-Gilman (ALICE), in *59th Rencontres de Moriond on QCD and High Energy Interactions: Moriond QCD 2025* (2025) arXiv: 2506.22692[nucl-ex].
[26] V. Chekhovsky *et al*., Phys. Lett. B **866**, 139556 (2025), arXiv: 2503.19993[nucl-ex]
[27] A. Hayrapetyan *et al*., Phys. Rev. Lett. **133**, 071903 (2024), arXiv: 2402.13864[hep-ex]
[28] K. Devereaux, W. Fan, W. Ke *et al*., arXiv: 2303.08143[hep-ph]
[29] Y. Fu, B. Müller, and C. Sirimanna, arXiv: 2411.04866[nucl-th]
[30] J. A. Barata, Z.-B. Kang, X. Mayo López *et al*., arXiv: 2411.11782[hep-ph]
[31] A. Nambrath, in *12th International Conference on Hard and Electromagnetic Probes of High-Energy Nuclear Collisions: Hard Probes 2024*, arXiv: 2510.16195[nuclex]
[32] K.-M. Shen, S.-Y. Chen, Y.-J. Huang *et al*., arXiv: 2410.05081[hep-ph]
[33] J. a. Barata and Y. Mehtar-Tani, PoS HardProbes **2023**, 145 (2024), arXiv: 2307.08943[hep-ph]
[34] S.-Y. Chen, Z.-X. Xu, K.-M. Shen *et al*., arXiv: 2409.13996[nucl-th]
[35] J. Barata, M. V. Kuzmin, J. G. Milhano *et al*., Phys. Rev. D **112**, 016005 (2025), arXiv: 2412.03616[hep-ph]
[36] H. Bossi, A. Kudinoor, I. Moult *et al*., arXiv: 2509.08047[hep-ph]
[37] J. Barata, D. Frenklakh, and S. Mukherjee, arXiv: 2507.16890[hep-ph]
[38] W.-J. Xing, S. Cao, G.-Y. Qin *et al*., Phys. Rev. Lett. **134**, 052301 (2025), arXiv: 2409.12843[hep-ph]
[39] C. Andres, F. Dominguez, J. Holguin *et al*., Phys. Rev. D **110**, L031503 (2024), arXiv: 2307.15110[hep-ph]
[40] J. Barata, J. Brewer, K. Lee *et al*., arXiv: 2508.19404[hep-ph]
[41] C. Andres, F. Dominguez, R. Kunnawalkam Elayavalli *et al*., Phys. Rev. Lett. **130**, 262301 (2023), arXiv: 2209.11236[hep-ph]
[42] C. Andres, F. Dominguez, J. Holguin *et al*. JHEP **2023**, 088(2023), arXiv: 2303.03413[hep-ph]
[43] C. Andres, F. Dominguez, J. Holguin *et al*. JHEP 2025, 166(2025), arXiv: 2407.07936[hep-ph]
[44] Z. Yang, Y. He, I. Moult *et al*., Phys. Rev. Lett. **132**, 011901 (2024), arXiv: 2310.01500[hep-ph]
[45] H. Bossi, A. S. Kudinoor, I. Moult *et al*., JHEP **12**, 073 (2024), arXiv: 2407.13818[hep-ph]
[46] C. Andres, F. Dominguez, J. Holguin *et al*., arXiv: 2411.15298[hep-ph]
[47] L. Apolinário, R. Kunnawalkam Elayavalli, N. O. Madureira *et al*., Phys. Rev. D **112**, 054018 (2025), arXiv: 2502.11406[hep-ph]
[48] C. Andres, J. Holguin, R. Kunnawalkam Elayavalli *et al*., Phys. Rev. Lett. **134**, 082303 (2025), arXiv: 2409.07514[hep-ph]
[49] C. Andres and J. Holguin, arXiv: 2409.07526 [hep-ph]
[50] J. Barata, I. Moult, A. V. Sadofyev *et al*., arXiv: 2503.13603[hep-ph]
[51] K. Lee and I. Moult, arXiv: 2308.00746[hep-ph]
[52] Y.-T. Chien, A. Deshpande, M. M. Mondal *et al*., Phys. Rev. D **105**, L051502 (2022), arXiv: 2109.15318[hep-ph]
[53] X.-N. Wang *et al*., eds., *New Opportunities in Particle and Nuclear Physics with Energy Correlators*, Central China Center for Nuclear Theory (Central China Center for Nuclear Theory (C3NT), 2025) two-week program with special symposium on May 17th celebrating C3NT inauguration.
[54] G. Marchesini, Nucl. Phys. B **445**, 49 (1995), arXiv: hepph/9412327
[55] P. T. Komiske, I. Moult, J. Thaler *et al*., Phys. Rev. Lett. **130**, 051901 (2023), arXiv: 2201.07800[hep-ph]
[56] D. Neill, G. Vita, I. Vitev *et al*., arXiv: 2203.07113[hep-ph]
[57] T. Sjöstrand, S. Ask, J. R. Christiansen *et al*., Comput. Phys. Commun. **191**, 159 (2015), arXiv: 1410.3012[hep-ph]
[58] P. Skands, S. Carrazza, and J. Rojo, Eur. Phys. J. C **74**, 3024 (2014), arXiv: 1404.5630[hep-ph]
[59] M. R. Aguilar, Z. Chang, R. K. Elayavalli *et al*., Phys. Rev. D **105**, 016011 (2022), arXiv: 2110.09447[hep-ph]
[60] M. Cacciari, G. P. Salam, and G. Soyez, JHEP **04**, 063 (2008), arXiv: 0802.1189[hep-ph]
[61] J. Yan, S.-Y. Chen, W. Dai *et al*., Chin. Phys. C **45**, 024102 (2021), arXiv: 2005.01093[hepph]
[62] S.-Y. Chen, J. Yan, W. Dai *et al*., Chin. Phys. C **46**, 104102 (2022), arXiv: 2204.01211[hepph]
[63] W. Dai, M.-Z. Li, B.-W. Zhang *et al*., arXiv: 2205.14668[hep-ph]
[64] Y. Li, S. Wang, and B.-W. Zhang, Phys. Rev. C **108**, 024905 (2023), arXiv: 2209.00548[hep-ph]
[65] S. Wang, Y. Li, J.-W. Kang *et al*., arXiv: 2408.10924[hep-ph]
[66] Y. Li, S.-Y. Chen, W. Kong *et al*., arXiv: 2409.12742[hep-ph]
[67] B. Alver, M. Baker, C. Loizides *et al*., arXiv: 0805.4411[nucl-ex]
[68] R. B. Neufeld, Phys. Rev. D **83**, 065012 (2011), arXiv: 1011.4979[hep-ph]
[69] F. Cooper and G. Frye, Phys. Rev. D **10**, 186 (1974)
[70] J. Casalderrey-Solana, D. Gulhan, G. Milhano *et al*., JHEP 0 **3**, 135 (2017), arXiv: 1609.05842 [hep-ph]
[71] A. Majumder, Phys. Rev. D **85**, 014023 (2012), arXiv: 0912.2987[nucl-th]
[72] X.-F. Guo and X.-N. Wang, Phys. Rev. Lett. **85**, 3591 (2000), arXiv: hep-ph/0005044
[73] B.-W. Zhang and X.-N. Wang, Nucl. Phys. A **720**, 429 (2003), arXiv: hep-ph/0301195
[74] S. Cao, T. Luo, G.-Y. Qin *et al*., Phys. Lett. B **777**, 255 (2018), arXiv: 1703.00822[nucl-th]
[75] C. Shen, Z. Qiu, H. Song *et al*. Comput. Phys. Commun. **199**, 61 (2016), arXiv: 1409.8164[nucl-th]
[76] J. H. Putschke *et al*., arXiv: 1903.07706